Plasma Phys. Control. Fusion **50** (2008) 035011 (10pp) doi:10.1088/0741-3335/50/3/035011

Investigation of competitive oscillations between drift mode and flute mode in linear cylindrical ECR plasma

K Kamataki[1], S-I Itoh[2], Y Nagashima[2], S Inagaki[2], S Shinohara[1], M Yagi[2], T Yamada[2], Y Kawai[2], A Fujisawa[3] and K Itoh[3]

[1] Interdisciplinary Graduate School of Engineering Science, Kyushu University, Kasuga, Fukuoka 816-8580, Japan
[2] Research Institute for Applied Mechanics, Kyushu University, Kasuga, Fukuoka 816-8580, Japan
[3] National Institute for Fusion Science, Toki, Gifu 509-5292, Japan

E-mail: kamataki@riam.kyushu-u.ac.jp

Received 28 November 2007, in final form 10 January 2008
Published 14 February 2008
Online at stacks.iop.org/PPCF/50/035011

Abstract

A competitive coexistence between a drift mode and a flute mode has been investigated experimentally in a bounded cylindrical electron cyclotron resonance (ECR) plasma. This competitive cycle was repeated during a whole continuous discharge. Competitive phenomena appeared in plasmas when the density scale length was close to the critical value: the drift mode is dominant and the flute mode is suppressed just below a critical value, but above this value, the flute mode grows abruptly and the drift mode is suppressed. In this phase, the density gradient increases temporally. A small crash takes place when the density scale length reaches a limit value, and then the density profile goes back to the previous states and thus the drift mode is excited and the flute mode is suppressed. The direct nonlinear coupling between the drift mode and the flute mode is weaker than the process of the second harmonic generation of each mode, suggesting that the growth and decay of them are closely related to the modification of the radial density profile.

(Some figures in this article are in colour only in the electronic version)

1. Introduction

The plasma transport across the magnetic field is strongly affected by low frequency fluctuations, e.g. the drift wave instability, the frequency of which is much lower than the ion cyclotron frequency [1]. The nonlinear self-regulation mechanism of drift wave turbulence has been the subject of attention in order to understand the structural formation of plasma turbulence (see, e.g. reviews [2, 3]). The fluctuations in the range of drift wave frequencies are destabilized by dissipative and/or reactive instabilities. The former is, for example, the

collisional drift mode and the dissipative trapped electron instability and the latter instabilities include the flute (interchange) mode and the ion-temperature-gradient mode instability [4]. The coupling between dissipative and reactive instabilities has attracted attention in studies of the magnetic confinement devices [5, 6]. Thus, the coupling between the collisionless drift wave ($n \neq 0$) and convective cells ($n = 0$) has been investigated theoretically in a three-dimensional plasma model [7–10], where n is the toroidal mode number. However, the experimental observation of the dissipative–reactive mode coupling has not been reported, as far as we know.

The drift modes have a universal feature, driven by a gradient in the equilibrium pressure profile. In low-β plasmas, drift modes have an electrostatic character, leading to perturbations of density and plasma potential, but not of the magnetic field. Drift modes are excited in the wide radial region, where the inverse density scale length exceeds the critical value, and propagate perpendicularly to the magnetic field (in the azimuthal direction). In the presence of the magnetic field gradient, the average magnetic curvature is responsible for an effective gravity, which makes the flute mode unstable. Komori *et al* observed the coexistence of the drift wave and the Rayleigh–Taylor instability in the collisionless plasma curved device [11]. Poli characterized the drift-interchange instabilities (with the characteristics of the drift waves destabilized in the unfavourable curvature region by an interchange mechanism) in the toroidal device TORPEX [12]. The combined effect of pressure gradient and effective gravity on the dispersion relation was investigated in [13, 14]. However, the dynamics of the coexistence between the drift and the flute modes have not been clarified as yet.

In the previous work [14], the authors reported the coexistence of the drift and flute modes in a linear cylindrical electron cyclotron resonance (ECR) plasma device. It was limited to the study of time average phenomena, e.g. an auto-power spectrum. In this paper we focus on the time evolution of both fluctuations to understand the dynamics of the coexistence between these two modes, and report the first observation of the competitive state between the drift mode and the flute mode, and discuss the nonlinear coupling of them.

The paper is organized as follows. The experimental setup including the diagnostic method is presented in section 2. Section 3 deals with the experimental results of the competition behaviour between the drift and flute modes, and the discussion and summary of this study are given in sections 4 and 5.

2. Experimental setup

The experiments have been carried out on a bounded linear ECR plasma device [14], as shown in figure 1(*a*). The cylindrical vacuum chamber is made up of stainless steel with an inner diameter of 40 cm and an axial length L of 120 cm. Argon gas is fed into the vacuum chamber at $z = 30$ cm using a mass flow controller. Here, z is the distance from the boundary of the cylindrical vacuum chamber and a coaxial waveguide converter (inner diameter $= 10$ cm and $L = 21$ cm). The chamber is evacuated to a base pressure of less than 10^{-7} Torr using a rotary pump and a 1000 l s^{-1} turbo molecular pump (working pressure is $p_{(\mathrm{Ar})} = (0.2\text{–}2.0) \times 10^{-3}$ Torr). Eight magnetic coils (axial width is 6.4 cm in the z-direction and the outer diameter is 71.5 cm) form a mirror magnetic field. A microwave with a frequency of 2.45 GHz and an output power of $P_\mu \leqslant 1$ kW is launched into a chamber as a circular TE_{11} mode through the coaxial waveguide converter. The reflected power is reduced by a three-stub tuner and a movable metal plate in the coaxial waveguide. The axial boundary condition is determined from both ends of the vacuum chamber (terminated by a metal flange).

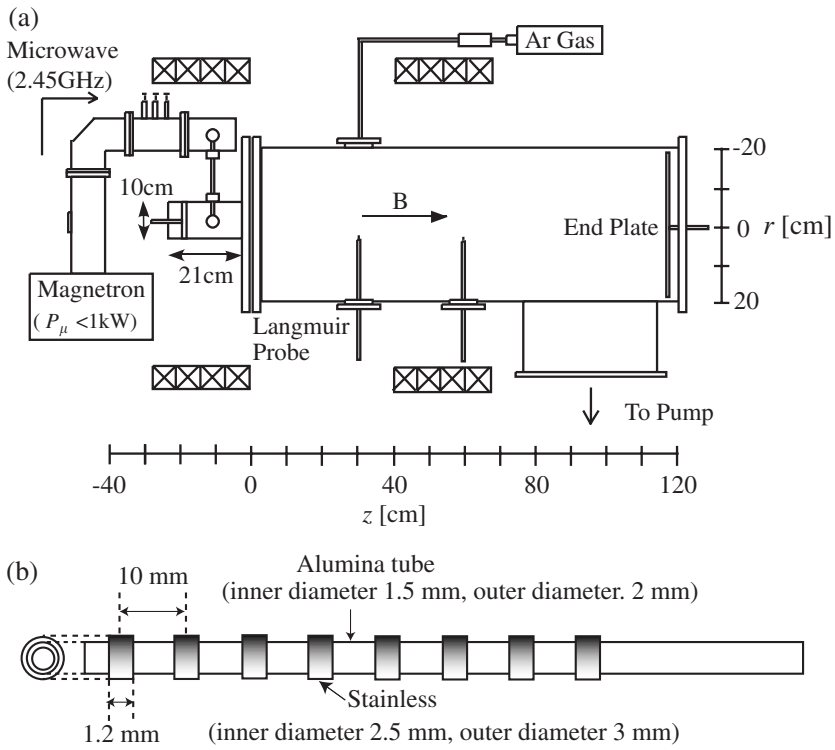

Figure 1. (*a*) Schematic diagram of the experimental setup and (*b*) the eight ring types probe array.

The plasma fluctuations (ion saturation current I_{is} and floating potential V_f) are measured with the Langmuir probes (a tungsten tip 1 mm in diameter and 2 mm in length). Time traces of I_{is} and V_f signals are recorded by a data logger with a sampling rate of 1 MHz (16 bit). The Langmuir probes are set at eight azimuthal positions and five axial positions. The azimuthal mode number m, parallel wave number n and azimuthal phase velocity can be determined from these measurements. Here, $n = 1$ indicates that the half wavelength is the same as the device length. In addition, in order to measure the spatio-temporal structures, we have developed a multi-channel Langmuir probe array. The array has stainless-steel rings (outer diameter of 3 mm, inner diameter of 2.5 mm and length of 1.2 mm with radial central separation of 10 mm) positioned in the radial direction, which are based on an alumina tube (outer diameter of 2 mm, inner diameter of 1.5 mm and length of 200 mm) (shown in figure 1(*b*)). Here, the same type of probe array in a toroidal plasma device is shown in [15]. Both, the time-averaged and the fluctuated radial density gradients are determined from this probe array using the least square method at the adjacent three radial positions.

Typical plasma parameters are as follows: electron density $n_e \sim 10^{11}\,\mathrm{cm}^{-3}$, electron temperature $T_e \sim 2\,\mathrm{eV}$ and plasma potential $V_p \sim 15\,\mathrm{V}$. These are obtained from current–voltage (I–V) characteristics of the Langmuir probe. In this operational regime, the dominant collisional process is the ion–neutral particle collision; here, the ion–neutral collision frequency ν_{in} is $\sim 1.6 \times 10^4\,\mathrm{s}^{-1}$. Here, the experimental conditions are as follows: the measurement point of $z = 30\,\mathrm{cm}$ and $r = 3\,\mathrm{cm}$ with $P_\mu = 300\,\mathrm{W}$ and magnetic field strength $B = 685\,\mathrm{G}$ (unless specified).

3. Experimental results

3.1. Coexistence of drift mode and flute mode

In this linear plasma, both the drift mode and the flute mode are excited in a particular neutral pressure region [14]. Here, both (the drift mode ($m/n = 4/1$) and the flute mode ($m/n = 2/0$)) were identified from the measurement of the axial and the azimuthal wave numbers, phase differences between density and potential fluctuations and the comparison between normalized amplitudes of density and potential fluctuations. Figure 2(d) shows the amplitude of both modes as a function of the neutral pressure, which is used as an index of the collisional damping of each mode. In the lower filling gas pressure regime (state 1), the drift mode is excited but the flute mode is stabilized. The density, its gradient and its inverse scale length increase with increase in the pressure. In the higher pressure regime (state 3), the flute mode is excited and only the drift mode is stabilized. In an intermediate regime (state 2), the drift mode is gradually suppressed and the flute mode becomes unstable and thus both modes are coexistent. The critical value of the inverse gradient scale length, above which the flute mode is excited, is $\sim$0.4 cm^{-1}. A linear stability analysis using the Hasegawa–Wakatani model gives similar growth rates of both modes in this coexistence condition [14]. Figures 2(a)–(c) show that the density ($I_{\rm is} \propto n_{\rm e}$), its gradient ($-{\rm d}I_{\rm is}/{\rm d}r \propto \nabla n_{\rm e}$) and its inverse scale length ($\nabla n/n$) change drastically in state 2. State 2 is considered to be a meso-state for a smooth transition from state 1 to state 3.

In fact, state 2 is a non-stationary state. Figures 3(a), (c) and (e) show typical time evolutions of $I_{\rm is}$ in each of the states. The fluctuation levels of $I_{\rm is}$ in states 1 and 3 are almost constant with time. On the other hand, $I_{\rm is}$ repeated the rise and the drop in a certain period in state 2. In particular, this repetition of $I_{\rm is}$ is clearly shown in figures 3(e) and (g), which indicates that a relaxation of the global parameter takes place. Typical frequency spectra of $I_{\rm is}$ in each state are shown in figures 3(b), (d) and (f). Two peaks with frequency f of $\sim$4.5 kHz in figure 3(b) and of $\sim$4 kHz in figure 3(f) were identified as drift wave. The other two peaks with $f = 1$–2 kHz in figures 3(d) and (f) were identified as the flute mode. Figure 3(g) shows the enlarged view of an equilibrium quantity $I_{\rm is0}$ (black line) of figure 3(e) for 0.2–0.6 s. It is found that there are two phases for one period in the coexistent modes: state 2 is divided into phase A and phase B, as indicated by the vertical dashed lines. In phase A, $I_{\rm is0}$ grows very slowly (the increasing rate is 0.16 s^{-1}). At the beginning of phase B, $I_{\rm is0}$ rises abruptly (the increasing rate is $\sim$1.7 s^{-1} at $t \sim 0.42$ s). At the end of phase B, $I_{\rm is}$ reaches a certain maximum value, and then a crash takes place, and after that, phase A starts again. Figure 3(h) shows the frequency spectra in phase A (red line) and phase B (blue dashed line): in phase A, the power of the drift mode with $f \sim 4$ kHz is larger than that of the flute mode with $f \sim 2$ kHz. On the other hand, the power of the flute mode is larger than that of the drift mode in phase B. It is found that a change in the dominant mode is observed between phase A and phase B. The coexistent state of the drift and the flute modes is realized by a competitive oscillation between them.

3.2. Competition between drift mode and flute mode

Figure 2 shows that the density, its gradient, its inverse scale length and the squared amplitude of each mode change gradually when the neutral pressure increases. However, the density and the power of each mode can vary in a short time scale as shown in figures 3(g) and (h). Thus, the profiles also change abruptly. Figure 4 shows a comparison of the amplitudes of the drift mode ($f \sim 3.8$–4.3 kHz), the flute mode ($f \sim 1.5$–2.0 kHz), radial profiles of $I_{\rm is}$, $-{\rm d}I_{\rm is}/{\rm d}r$ and the inverse density gradient scale length $\nabla n/n$ between phase A and phase B.

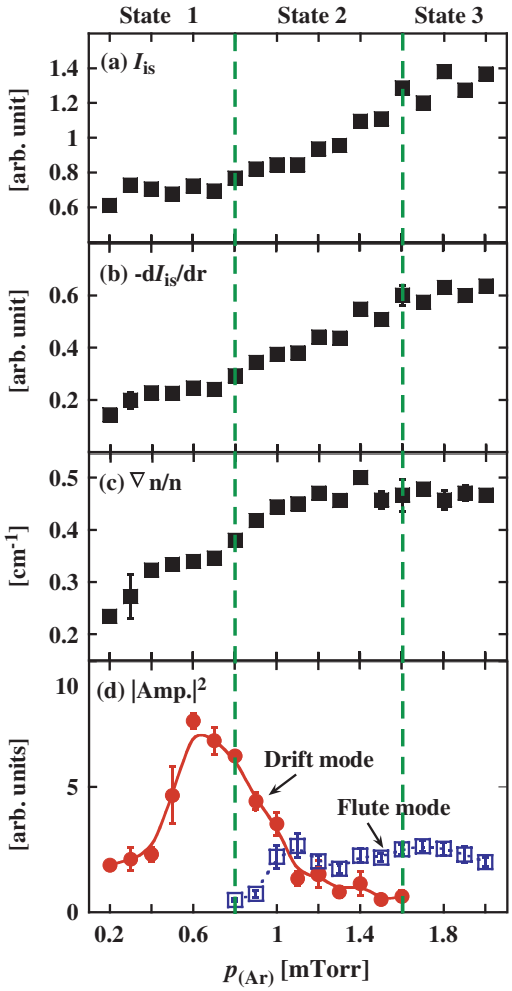

Figure 2. Dependence of (*a*) time-averaged ion saturation current, (*b*) time-averaged radial density gradient, (*c*) time-averaged gradient scale length and (*d*) square of drift and flute modes' fluctuation amplitude on the neutral gas pressure including the line dividing operation regions into states 1–3.

Here, radial profiles are measured with the ring probe array. In phase A, the drift mode is larger than the flute mode in all radial positions. In phase B, the flute mode is larger than the drift mode in all radial positions. Namely, the dominant modes in phase A and phase B are the drift and the flute modes, respectively, and have peaks near the same radial position ($r = 3$ cm). I_{is} in phase B is slightly larger than that in phase A in the region of $r \leqslant 4$ cm. $-\mathrm{d}I_{is}/\mathrm{d}r$ in phase B is also slightly larger than that in phase A, particularly in the region of $r = 2$–3 cm. $\nabla n/n$ in phase B are larger than that in phase A except at $r < 2$ cm. Differences in these profiles are small; however, the changes in the mode amplitude are significant. Thereby, a critical profile exists, and thus the cyclic competitive process of the drift–flute mode is considered to be a repetition of forward–backward transition (from phase A to phase B and reverse) around the critical profile. In order to clarify the coupling mechanism among the drift mode the flute mode and the density profile, we focus on the temporal behaviour of both modes at $r = 3$ cm.

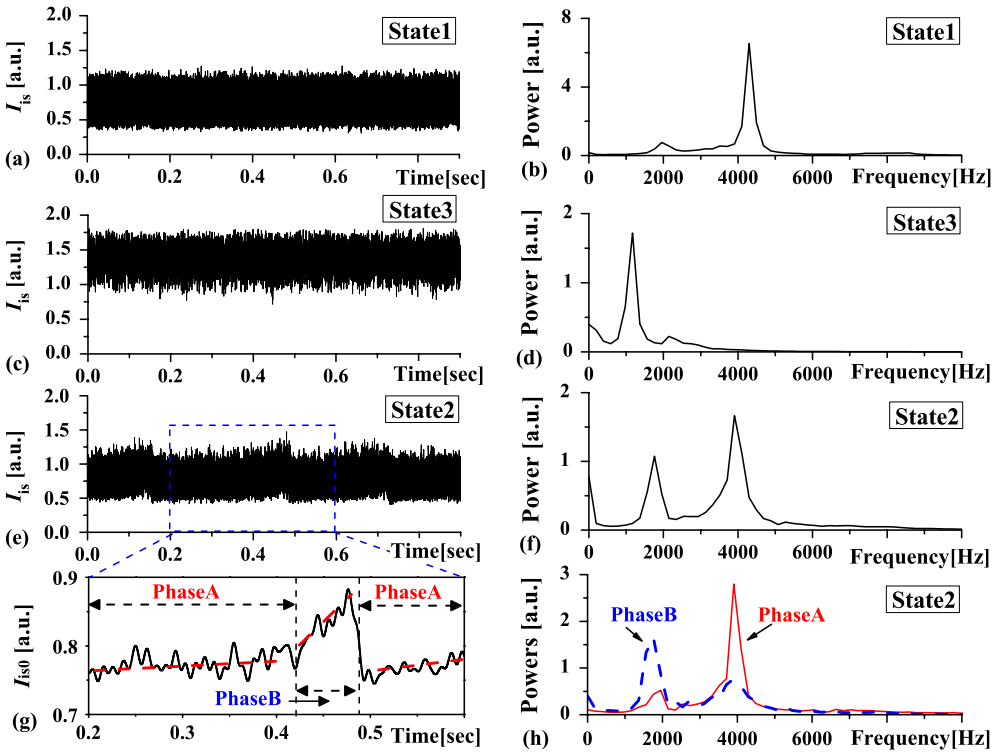

Figure 3. Time evolutions of I_{is} in (*a*) state 1, (*c*) state 3 and (*e*) state 2 and frequency spectra in (*b*) state 1, (*d*) state 3 and (*f*) state 2. Inset (*g*) is an enlarged view of an equilibrium quantity I_{is0} (black line) of figure 3(*e*) (using a low pass filter, $f < 100$ Hz) in 0.2–0.6 s, including vertical black dashed lines, which divide state 2 into phase A and phase B: the increasing rate of I_{is0} (red dashed lines) in phase A is smaller than phase B. (*h*) Frequency spectra in phase A (red line) and phase B (blue dashed line) in state 2 are also shown.

The envelope analysis of each mode is useful to discuss the dynamics of waves. The time evolutions of I_{is0}, $-\mathrm{d}I_{is}/\mathrm{d}r$, $\nabla n/n$ and the envelopes of the fluctuation intensity, which are the flute mode (1.5–2.0 kHz) and the drift mode (3.8–4.3 kHz) measured using the band-pass filter at $r = 3$ cm, are shown in figure 5. In phase A, the drift mode stays with a higher amplitude without flute mode excitation and I_{is} and $-\mathrm{d}I_{is}/\mathrm{d}r$ grow very slowly. When $-\mathrm{d}I_{is}/\mathrm{d}r$ or $\nabla n/n$ exceeds a critical value, the flute mode begins to grow abruptly (phase B). The drift mode is suppressed by flute–drift mode coupling, and thus the $-\mathrm{d}I_{is}/\mathrm{d}r$ increases. Finally, when I_{is} and $-\mathrm{d}I_{is}/\mathrm{d}r$ reach a limit at the end of phase B, the crash of I_{is} and $-\mathrm{d}I_{is}/\mathrm{d}r$ takes place and it leads to the decay of the flute mode and the excitation of the drift mode. These suggest that the abrupt growth of the perturbations leads to crashes, and the saturation of both mode fluctuations is correlated with the modifications of I_{is} and $-\mathrm{d}I_{is}/\mathrm{d}r$. Figure 5(*d*) shows the ratio of the drift mode amplitude to the total amplitude (Ratio $=$ Env.$_{\mathrm{D}}$/(Env.$_{\mathrm{D}}$ + Env.$_{\mathrm{F}}$)) and envelopes of the flute and the drift modes. Here Env.$_{\mathrm{D(F)}}$ indicates the amplitude of the drift (flute) mode from the envelope analysis. This result shows the ratio that the drift mode exists is large in phase A. Figures 5(*g*) and (*h*) show the probability distribution functions (PDFs) of the envelopes of the drift mode and the flute mode. These PDFs are asymmetric. The PDF of the flute mode has a positive tail. On the other hand, the PDF of the drift mode has a negative tail. This indicates that there are two

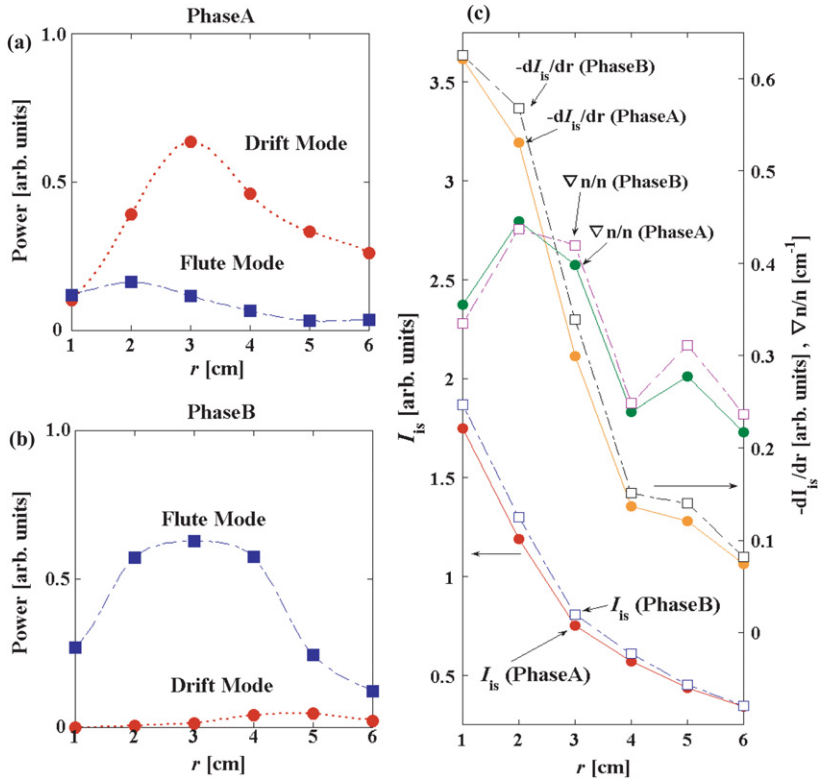

Figure 4. (*a*) and (*b*) Amplitudes of the drift mode and the flute mode and radial profiles of (*c*) $I_{\rm is}$, $-{\rm d}I_{\rm is}/{\rm d}r$ and $\nabla n/n$ in phase A and phase B.

stable states in each mode and a seesaw relationship between the stable modes. The cross correlation factor between the envelopes of the drift and the flute modes is high and negative (~ -0.6) in this whole discharge. The transition of each mode may be coupled. The repetition period in the cyclic phenomena is considered to be related to the density build-up time. The time scale of the crash ($\sim$0.02 s) is much smaller than that of the build-up time of the electron density ($\sim$0.3 s).

4. Discussion

The drift–flute competition process involves the density profile. To explain the competition process, the direct coupling between the drift and the flute modes and/or the further interaction mechanism between both modes and the density profile are important. Here, we investigate the direct nonlinear interaction between the drift and the flute modes and other components by using the bicoherence analysis [16].

Many Fourier components are excited in plasmas, and the broad-band higher frequency tail in the spectrum can be described by the energy transfer away from an initially unstable mode via three-wave interactions. A measure of the statistical dependence between three waves is given by the bispectrum, which is given, for example, for density fluctuations, by the ensemble average

$$\hat{B}(\omega_1, \omega_2) = \langle X(\omega_1) X(\omega_2) X^*(\omega_1 \pm \omega_2) \rangle, \tag{1}$$

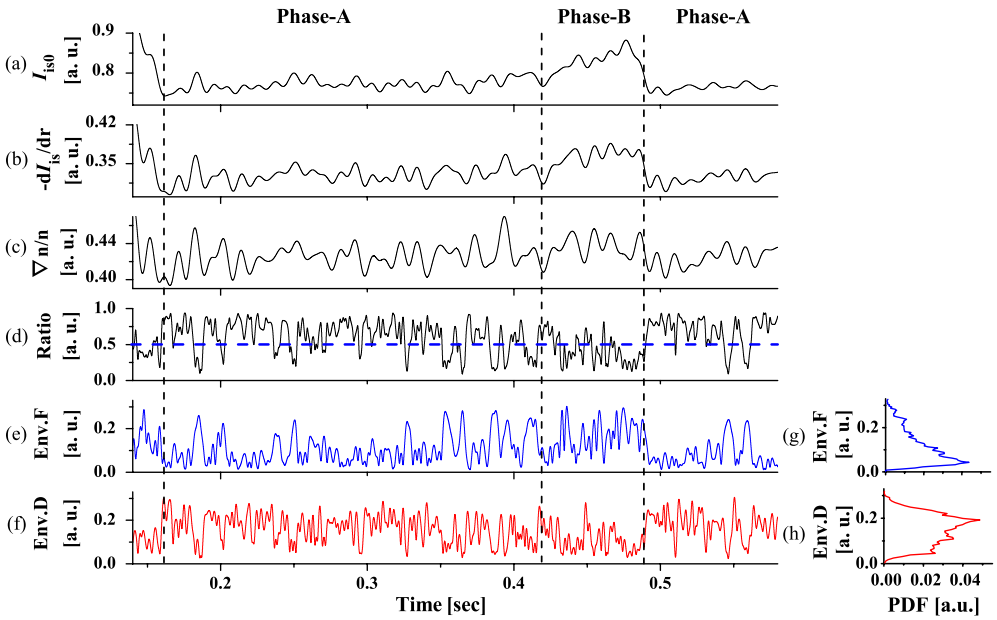

Figure 5. Time evolutions of (*a*) I_{is0}, (*b*) $-\mathrm{d}I_{is}/\mathrm{d}r$, (*c*) $\nabla n/n$, (*d*) the ratio of the drift mode and envelopes of (*e*) the flute mode and (*f*) the drift mode. (*g*)–(*h*) The PDFs of (*e*) and (*f*).

where $X(\omega_n)$ and $\langle\,\rangle$ indicate a Fourier component at ω_n and the ensemble average, respectively. The bispectrum analysis can clarify the three-wave nonlinear interaction under the condition that $\omega_1 + \omega_2 = \omega_3$ and $k_1 + k_2 = k_3$, where $\omega_{1,2,3}$ and $k_{1,2,3}$ are frequencies and wave numbers of the three waves, respectively.

A quantitative measure of the phase coherence can be made by computing the bicoherence spectrum, which is defined in terms of the bispectrum as

$$\hat{b}^2(\omega_1, \omega_2) = \frac{|\hat{B}(\omega_1, \omega_2)|^2}{\langle |X(\omega_1)X(\omega_2)|^2\rangle \langle |X(\omega_1 \pm \omega_2)|^2\rangle}, \tag{2}$$

where $\hat{b}^2(\omega_1, \omega_2)$ will take a value close to unity (indicating a high degree of phase coherence) when a nonlinear (strictly speaking, quadratic) interaction has taken place. On the other hand, a value of $\hat{b}^2(\omega_1, \omega_2)$ which is near zero (low degree of phase coherence) shows the absence of quadratic nonlinearity and thus any waves present at $\omega_{1,}\omega_2$ and $\omega_1 + \omega_2$ are spontaneously excited independent modes rather than (quadratically) coupled modes.

Here, the nonlinear interaction between the drift and the flute modes and the others is analysed by the above bicoherence analysis. Figure 6 shows the result of the squared auto-bicoherence of I_{is}. There are three distinctive features. First, there is a noticeable peak at the frequency of the drift mode, $f \sim 4$ kHz. The peaks are seen at $f_1 \sim 4$ kHz, $f_2 \sim \pm 4$ kHz and $f_1 + f_2 = f_3 = \pm 4$ kHz. These peaks indicate a strong nonlinear interaction between the drift mode and the higher frequency broad-band fluctuations which are more than ∼8 kHz. In addition, the magnitude of the squared auto-bicoherence (at these peaks) has a weak dependence on frequencies f_1 and f_2. The second feature is that strong squared auto-bicoherence is observed at $f_1 \sim 1.8$ kHz, $f_2 \sim \pm 1.8$ kHz and $f_1 + f_2 = f_3 = \pm 1.8$ kHz. These peaks show a strong nonlinear interaction between the flute mode

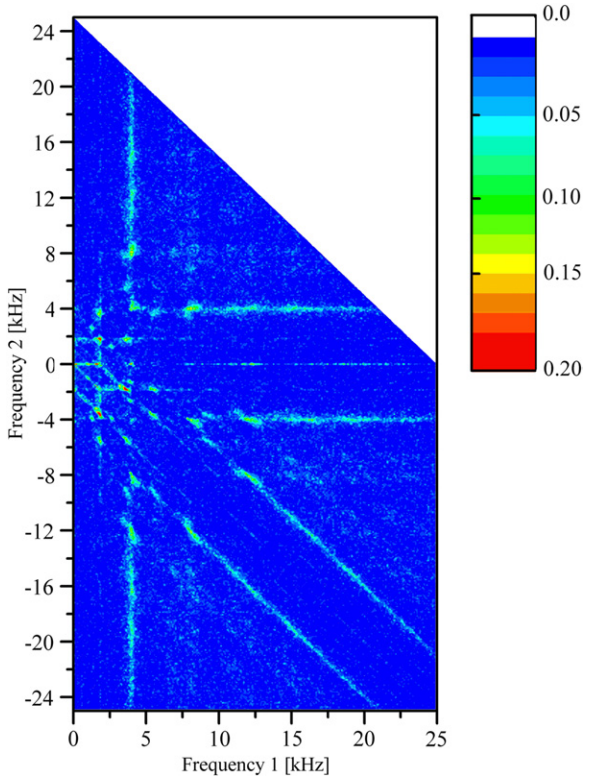

Figure 6. Squared auto-bicoherence plane of I_{is}.

and the lower frequency broad-band fluctuations which are less than ∼3.6 kHz. The third feature is that a small but finite squared auto-bicoherence is observed at $f_1 \sim 1.8$ kHz, $f_2 \sim \pm 4$ kHz and $f_1 + f_2 = f_3 = -2.2, +5.8$ kHz. This shows the weak nonlinear interaction between the drift mode and the flute mode. Here, $\hat{b}^2$ ($f_3 = -2.2$ kHz) is about one-fifth of $\hat{b}^2$ ($f_3 = -1.8$ kHz) and about one-third of $\hat{b}^2$ ($f_3 = -4$ kHz). These results show that the direct interaction effects between the drift and flute modes (e.g. energy transfer) are smaller than the process that the drift modes (or flute mode) generates the second harmonics.

Summarizing these results, the flute mode generates the second harmonics and has a direct interaction with broad-band components which are less than ∼3.6 kHz. The drift mode also generates the second harmonics and has a strong nonlinear interaction with broad-band components more than ∼8 kHz. Though the drift and the flute modes are coexistent in the auto-power spectrum X (ω_n), the direct interaction between them is not strong. It comes from the dynamics of the drift and flute modes growing alternately in time evolutions. Interaction mechanisms between the drift and/or the flute mode and the density profile may be more important. In particular, the crash mechanism is still unknown. When the ion saturation current drops abruptly in the central region, it increases simultaneously outside, which suggests that the central density transports outside. This will be reported in a future work. Convincing theoretical models, which can explain the seesaw relationship between the drift and the flute modes and the density crash, are strongly required.

5. Summary

In this paper, we have reported competitive oscillations between the drift instability and the flute instability in a linear cylindrical ECR plasma device. A successive excitation of drift and flute instabilities is observed and a cyclic competition process was revealed by the envelope analysis. The competition process is as follows: (1) the drift mode is excited with a suppression of the flute mode, and n_e, ∇n_e and $\nabla n/n$ increase slowly. (2) When n_e, ∇n_e and $\nabla n/n$ exceed a critical value, the flute mode is excited with a suppression of the drift mode. (3) When n_e, ∇n_e and $\nabla n/n$ reach a limit, a crash takes place. The repetition period is considered to be related to the density build-up time. The auto-bicoherence analysis demonstrated that the drift mode is weakly nonlinearly coupled with the flute mode. That is, the direct interaction (e.g. the energy transfer) between both modes is small. The growth and decay of both modes are closely related to the modification of the radial density profile.

Acknowledgments

The authors wish to acknowledge fruitful discussions with Dr N Kasuya and Dr S Nishimura. This work is partially supported by a Grant-in-Aid for Specially-Promoted Research of MEXT of Japan (16002005) and by a collaborative program between the Research Institute for Applied Mechanics of Kyushu University and The National Institute for Fusion Science (NIFS) (NIFS07KOAP017).

References

[1] Kadomtsev B B 1965 *Plasma Turbulence* (New York: Academic)
[2] Itoh K, Itoh S-I and Fukuyama A 1999 *Transport and Structural Formation in Plasmas* (Bristol: Institute of Physics Publishing)
[3] Diamond P H, Itoh S-I, Itoh K and Hahm T S 2005 *Plasma Phys. Control. Fusion* **47** R35
[4] Horton W 1999 *Rev. Mod. Phys.* **71** 735
[5] Scott B D 2005 *Phys. Plasma* **12** 62314
[6] Kadomtsev B B and Pogutse O P 1970 *Reviews of Plasma Physics* vol 5 (New York: Consultants Bureau) p 249
[7] Cheng C Z and Okuda H 1977 *Phys. Rev. Lett.* **38** 708
[8] Sagdeev R Z and Galeev A A 1969 *Nonlinear Plasma Theory* (New York: Benjamin)
[9] Horton W 1984 Drift wave turbulence and anomalous transport *Basic Plasma Physics II* ed A A Galeev and R N Sudan (Amsterdam: North-Holland)
[10] Yagi M *et al* 1998 *Plasma Physics and Controlled Nuclear Fusion Research 19th IAEA Fusion Energy Conf. (Lyon, France, 2002)* (Vienna: IAEA) IAEA-CN-94/TH/1-4
[11] Komori A, Sato N and Hatta Y 1978 *Phys. Rev. Lett.* **40** 768
[12] Poli F M *et al* 2006 *Phys. Plasma* **13** 102104
[13] Perez J C *et al* 2006 *Phys. Plasma* **13** 32101
[14] Kamataki K *et al* 2007 *J. Phys. Soc. Japan* **76** 054501
[15] Muller S H *et al* 2005 *Phys. Plasma* **12** 090906
[16] Kim Y C and Powers E J 1979 *IEEE Trans. Plasma Sci.* **RS-7** 120